Journal of Medicinal Chemistry

pubs.acs.org/jmc Article

Examining Arginase-1 Trimerization Uncovers a Promising Allosteric Site for Inhibition

Juhans Dechenne, Magdalena Wierzbicka, Reda Krimou, Asia El Aakchioui, Julia Malo Pueyo, Joris Messens, Marianne Fillet, Quentin Spillier, and Raphaël Frédérick*

Cite This: J. Med. Chem. 2025, 68, 1433−1445 Read Online

ABSTRACT: Arginase-1 (ARG-1) is a promising target for cancer immunotherapy, but the small size and the highly polar nature of its catalytic site present significant challenges for inhibitor development. An alternative strategy to induce enzyme inhibition by targeting protein oligomerization has been developed recently, offering several advantages such as increased selectivity, promotion of protein degradation, and potential substoichiometric inhibition. In this study, we demonstrated that only trimeric ARG-1 is active, which was confirmed by producing monomeric arginase-1. Through *in silico*-driven site-directed mutagenesis, we identified an allosteric site involving five key amino acids responsible for ARG-1 trimerization. We further demonstrated the covalent modification of a key arginine residue within this pocket using phenylglyoxal disrupted ARG-1 oligomerization. Although phenylglyoxal has limited potency, it effectively supports the concept of ARG-1 inhibition via homomeric disruption, validating this allosteric targeting approach.

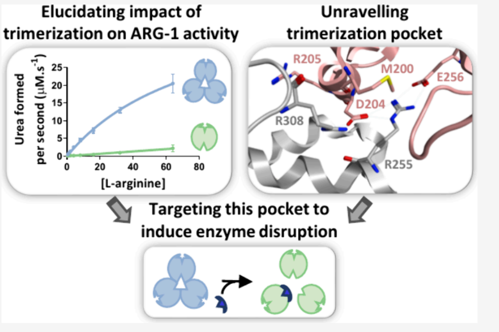

■ INTRODUCTION

In mammals, there are two different arginase (ARG) isoforms: arginase-1 (ARG-1) and arginase-2 (ARG-2). Both enzymes catalyze the conversion of L-arginine into urea and L-ornithine and share 58% sequence identity, with their active sites being 100% identical.[1] ARG-1 is primarily expressed in liver cytosol, whereas ARG-2 is found ubiquitously and is primarily expressed in the mitochondria. ARG-1 functions as a homotrimeric metalloenzyme, containing two essential Mn^{2+} ions in its active site.[2] This enzyme has emerged as an interesting therapeutic target due to its upregulation in multiple diseases,[3] notably in cardiovascular[4−10] and neurovascular diseases.[11−14] Furthermore, ARG-1 is involved in tumoral immune escape in multiple cancers such as head and neck cancers,[15] colorectal cancer,[16] ovarian carcinoma,[17] gastric cancer,[18] neuroblastoma,[19] acute myeloid leukemia,[20] breast cancer,[21] lung cancer,[22] thyroid cancer,[23] melanoma,[24] liver cancer,[25] renal cancer,[26] and glioblastoma,[27] where it was identified as a poor prognosis factor. ARG-1 is often overexpressed in myeloid-derived suppressor cells (MDSCs), which are recruited by cancer cells and secrete ARG-1 in the tumor microenvironment by exocytosis. This secretion decreases the extracellular L-arginine concentrations,[1] leading to reduced antitumor immune responses and promoting tumor growth and metastasis.[28]

Most of the reported ARG-1 inhibitors to date feature a reactive boronic acid function that targets the ARG-1 manganese-containing active site. Although potent, these compounds often suffer from poor selectivity and limited pharmacokinetic properties.[29,30] Despite this, two inhibitors, numidargistat and CB-280, have progressed into clinical studies for cancer treatment (phase 1/2) and cystic fibrosis (phase 1), respectively. Numidargistat has shown some antitumor efficacy *in vivo*, reducing tumor growth in models of colorectal carcinoma (CT26), breast cancer (4T1), melanoma (B16), and lung carcinoma (LLC), both as a single agent and in combination with immune checkpoint therapy.[31] However, no arginase inhibitors have yet been moved to the clinic.

To discover more selective ARG-1 inhibitors with improved pharmacokinetic profiles, we set out to investigate ARG-1 trimerization to identify novel targetable allosteric sites. Since ARG-1 trimers are the minimal functional units, ARG-1 activity depends on its oligomerization state. Targeting the oligomerization state of an enzyme is an emerging concept with promising potential.[32,33] Many proteins exhibit a homo-oligomeric state, forming functional, catalytically active, and stable protein complexes.[34−36] Some of these proteins are associated with pathological conditions, making them attractive therapeutic targets.[33] Targeting homomeric proteins with allosteric disrupters offers several advantages, including better

Received: August 21, 2024
Revised: December 13, 2024
Accepted: December 18, 2024
Published: January 2, 2025

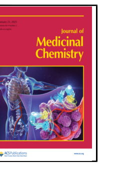

https://doi.org/10.1021/acs.jmedchem.4c01993
J. Med. Chem. 2025, 68, 1433−1445

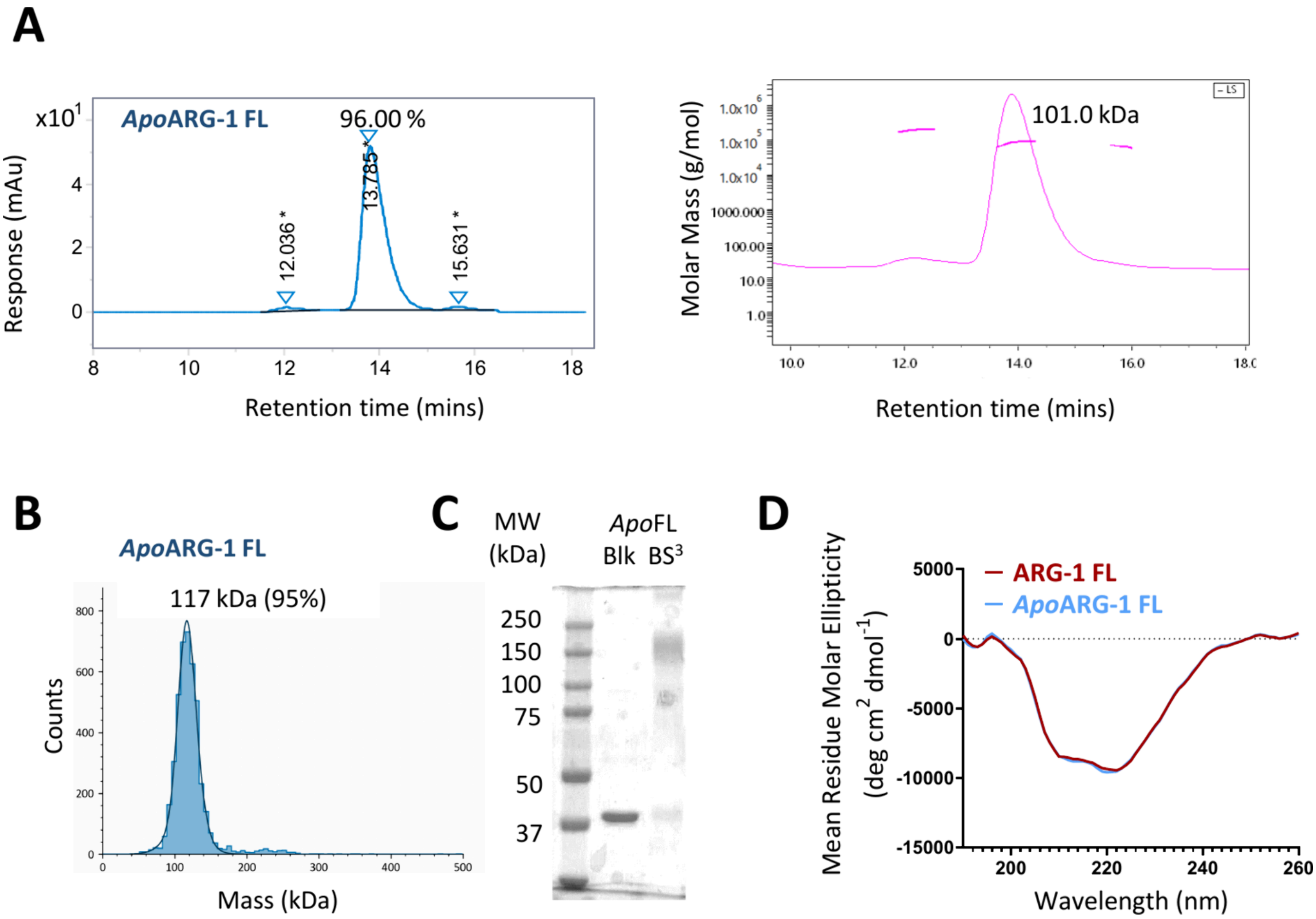

Figure 1. Cofactor Mn^{2+} is not essential for ARG-1 trimerization. (A) SEC-MALS experiment of *apo*ARG-1 FL (25 μM) with the calculated molecular weights of the complex in the solution and their relative intensity indicated above the peaks ($n = 3$). (B) Mass photometry experiment of *apo*ARG-1 FL (0.05 μM), with the calculated molecular weights of the complex in the solution and their relative intensity indicated above the peaks. (C) Cross-linking experiment of *apo*ARG-1 FL (4 μM) with BS^3 of 0.4 mM. (D) *Apo*ARG-1 FL and ARG-1 FL (0.2 mg/mL) CD spectra show similar secondary structures.

selectivity and reduced off-target effects,[37,38] increased protein degradation due to instability,[39,40] and the potential for substoichiometric inhibition.[41]

The crystal structure of ARG-1 highlights the importance of the S-shaped C-terminal tail in trimer stabilization.[42] Single-point mutation studies identified three amino acids (D204, E256, and R308) as essential for ARG-1 self-assembly. Mutating these residues to alanine or glutamine resulted in monomers[43−45] that lost up to 87% of their catalytic activity. Patients with missense mutations pArg308Gln[46] and nonsense mutations p.Arg291*[47,48] and p.Val293*[48] developed hyperargininemia due to defective ARG-1, attributed to disruptions in enzyme self-assembly, and prompted further exploration of ARG-1 homomeric disruption as a therapeutic strategy.

In this study, we established the essential role of trimerization in ARG-1 activity by producing and characterizing both a truncated monomeric model of ARG-1 (ARG-1 TR) and a full-length trimeric model of ARG-1 (ARG-1 FL). The oligomeric states were confirmed using three orthogonal methods: cross-linking, size-exclusion chromatography coupled with multiangle light scattering (SEC-MALS) and mass photometry. Furthermore, we identified an allosteric site comprising five critical amino acids involved in the self-assembly of ARG-1 through *in silico* studies and site-directed mutagenesis. We further demonstrated the potential of allosteric inhibition by covalently modifying an L-arginine residue within the identified pocket, thereby disrupting ARG-1 trimerization. Although this covalent binder has limited inhibitory potency, it serves as a promising chemical probe, highlighting the feasibility of this allosteric inhibition strategy.

RESULTS AND DISCUSSION

Mn^{2+} is Not Essential for ARG-1 Trimerization. Since previous studies have suggested that protein oligomerization can be regulated by their cofactor,[49−52] we first set out to investigate the role of Mn^{2+} for ARG-1 trimerization. To do this, we assessed the oligomeric state of *apo*ARG-1 FL, produced without Mn^{2+} at every step of the protein production, using SEC-MALS (Figure 1A), mass photometry (Figure 1B), and cross-linking (Figure 1C). These analyses revealed that *apo*ARG-1FL predominantly remained in a trimeric state, regardless of the method used (96% for the species at 101 kDa using SEC-MALS and 95% for the species at 117 kDa using mass photometry). These findings suggest that Mn^{2+} is not essential for trimerization, although it may still play a minor role, as evidenced by its slightly lower trimeric percentage compared to *holo*ARG-1 FL (98% using SEC-MALS and 100% using mass photometry, Figure 3). Additionally, circular dichroism experiments (CDs, Figure

https://doi.org/10.1021/acs.jmedchem.4c01993
J. Med. Chem. 2025, 68, 1433−1445

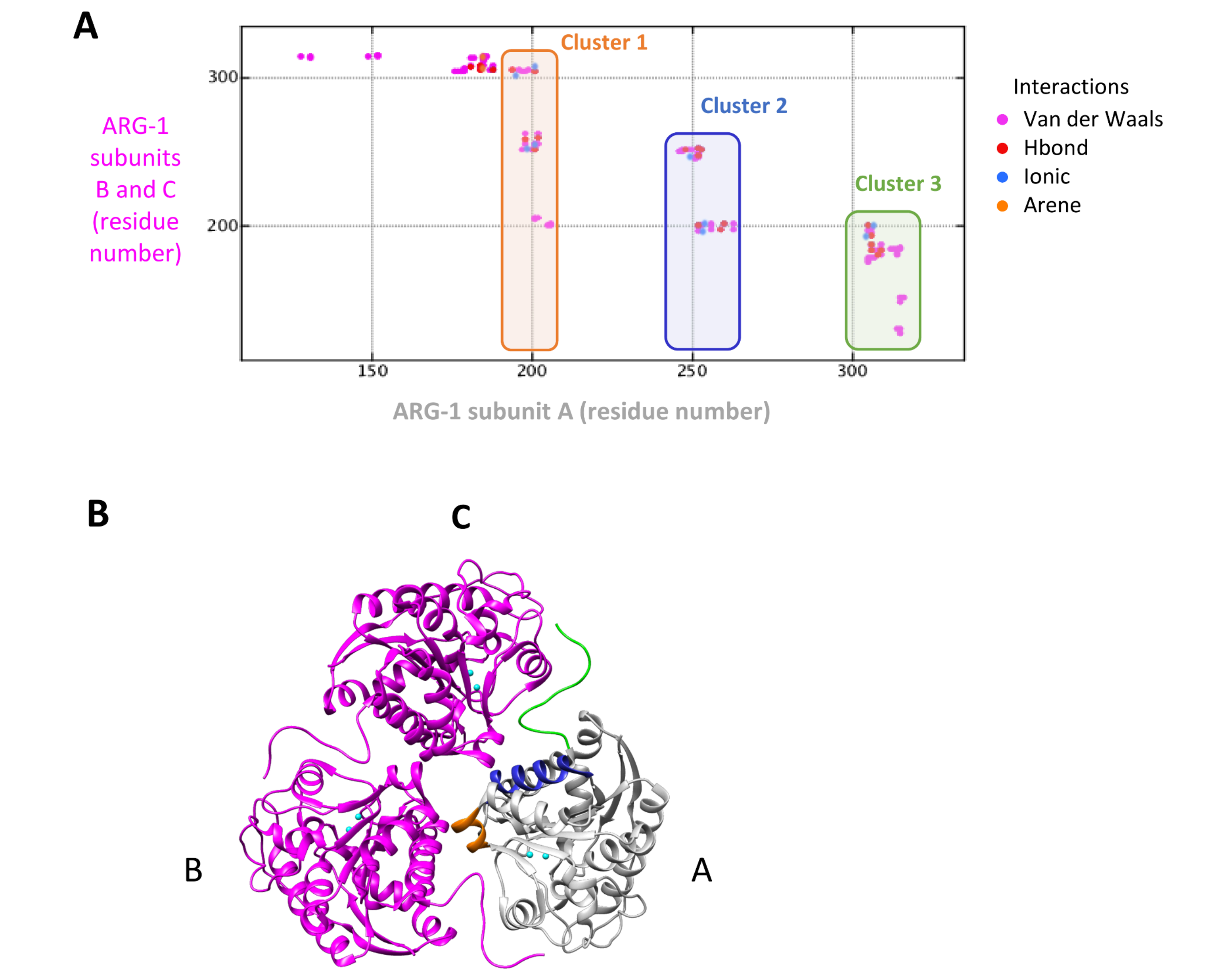

Figure 2. Epitope Mapping of ARG-1 self-assembly using *in silico* studies. (A) Mapping of the interactions between residues from ARG-1 subunit A and residues from subunits B and C using the Molecular Operating Environment software. (B) X-ray crystallographic structure of trimeric ARG-1 (PDB ID: 2AEB) with one monomer (subunit A, gray) colored differently from the two others (subunits B and C, magenta) and clusters 1, 2, and 3 identified using the MOE software colored respectively in orange, blue, and green.

1D) demonstrate that the secondary structure of ARG-1 is unaffected by Mn^{2+} incorporation, as similar spectra were obtained for *apo*ARG-1 FL and *holo*ARG-1 FL. Therefore, the study and characterization of monomeric arginase cannot rely on *apo*ARG-1, and using chelators is not an effective strategy to disrupt and inhibit ARG-1. Based on these results, we proceeded to identify the key hotspots responsible for this trimerization.

Production and Evaluation of Monomeric ARG-1. To validate our approach, we first demonstrated that monomeric ARG-1 leads to a significant loss of activity. *In silico* studies were conducted to identify specific regions responsible for ARG-1 trimerization and guide the design of monomeric ARG-1. Using the MOE software (ChemComp) and the trimeric ARG-1 structure (PDB entry 2AEB), we calculated the free binding energy between the amino acids of one monomer with those of the other two. Mapping the interactions between the residues of subunit A and those of subunits B and C (Figure 2A) revealed that the homomeric interface interactions are mainly nonpolar (van der Waals interactions), as expected for protein−protein interactions. However, hydrogen bonds (K155, P184, H187, K191, Y197, T201, D204, R205, G251, R255, E256, E262, E263, R308, E309, N311, H312, L318), ionic interactions (K191, D204, R205, R255, E256, E263, R308, E309), and $\pi-\pi$ stacking (Y188, H312, Y317) also play key roles in monomer interaction. We identified three main interaction clusters: cluster 1 (in orange, residues M200−L206), cluster 2 (in blue, residues T253-G268), and cluster 3 (in green, residues G305-Y322) (Figure 2A,B). Considering the established role of the C-terminal tail (cluster 3) in ARG-1 trimerization,[42] we strategically truncated the last 17 amino acids to generate a monomeric ARG-1, which we named ARG-1 TR.

The oligomeric states of ARG-1 TR (theoretical Mw of 34.9 kDa) and ARG-1 FL (theoretical Mw of 110.7 kDa) were first assessed using SEC-MALS. The results revealed that ARG-1 FL predominantly exists as a trimer (98% with a measured Mw of 112 kDa), as shown in Figure 3A. In contrast, ARG-1 TR primarily adopts a monomeric state (95% with a measured Mw of 37 kDa), as shown in Figure 3A. This observation was further confirmed by two orthogonal techniques: cross-linking (Figure 3B) and mass photometry (Figure 3C). It should be noted that for ARG-1 TR, mass photometry revealed a molecular weight closer to that of a dimer, likely due to

https://doi.org/10.1021/acs.jmedchem.4c01993
J. Med. Chem. 2025, 68, 1433−1445

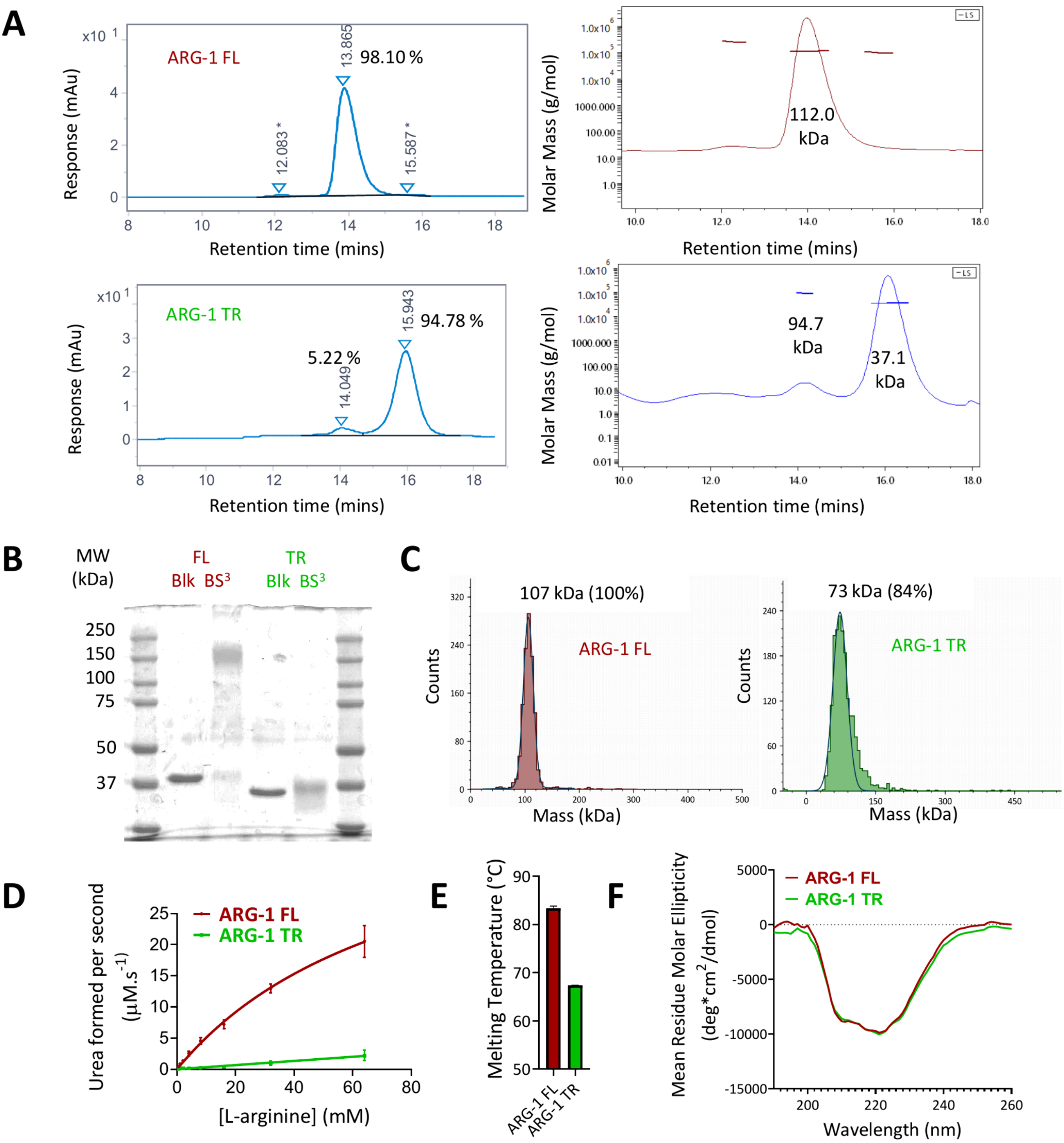

Figure 3. Comparison of ARG-1 FL and ARG-1 TR using different biochemical/biophysical tools. (A) SEC-MALS experiment of ARG-1 FL (25 μM) and ARG-1 TR (25 μM) with the calculated molecular weights of the complex in the solution and their relative intensity indicated above the peaks ($n = 3$). (B) Cross-linking experiment of ARG-1 FL (4 μM) and ARG-1 TR (4 μM) with BS^3 = 0.4 mM. (C) Mass photometry experiment of ARG-1 FL (0.05 μM) and ARG-1 TR (0.05 μM) with the calculated molecular weights of the complex in the solution and their relative intensity indicated above the peaks. (D) Evaluation of ARG-1 FL (0.1 μM) ($k_{cat}/K_M = 5.7 \times 10^3$ M^{-1} s^{-1}) and ARG-1 TR (0.1 μM) ($k_{cat}/K_M = 0.33 \times 10^3$ M^{-1} s^{-1}) activity under physiological conditions ($n = 6$). (E) Evaluation by nanoDSF of ARG-1 FL (10 μM, $T°_M$ = 83.4 °C) and ARG-1 TR (10 μM, $T°_M$ = 67.4 °C) melting temperatures ($n = 6$). (F) ARG-1 FL and ARG-1 TR (0.2 mg/mL) CD spectra show similar secondary structures.

method's detection limit (40 kDa).[53] Subsequently, we conducted enzyme assays under physiological conditions (pH 7.4, Mn^{2+} 0.2 μM[54,55]). This assay revealed that monomeric ARG-1 TR ($k_{cat}/K_M = 0.33 \times 10^3$ M^{-1} s^{-1}; Figure 3D, Table S1) experienced a substantial loss of activity (over 90%) compared to ARG-1 FL ($k_{cat}/K_M = 5.7 \times 10^3$ M^{-1} s^{-1}; Figure 3D and Table S1). This finding supports our initial hypothesis that disrupting the homomeric state of ARG-1 could be an effective strategy for enzyme inhibition. Moreover, it suggests that the hyperargininemia observed in patients with the

https://doi.org/10.1021/acs.jmedchem.4c01993
J. Med. Chem. 2025, 68, 1433−1445

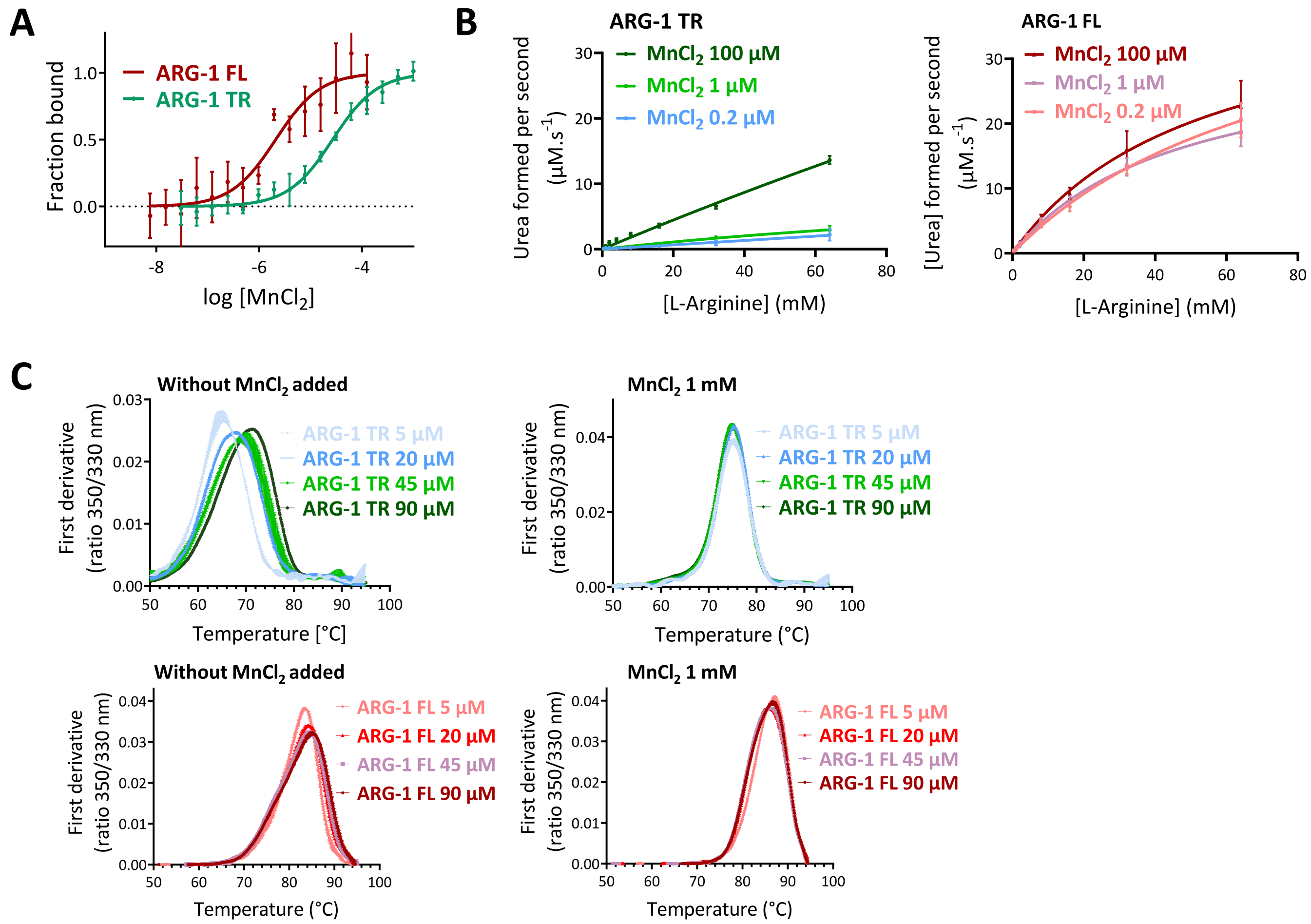

Figure 4. Monomeric ARG-1 loss of activity is linked to the loss of affinity for the cofactor Mn^{2+}. (A) Evaluation of *apo*ARG-1 FL (K_D = 1.07 μM) and *apo*ARG-1 TR (K_D = 20.16 μM) affinity for Mn^{2+} using MST (n = 3). (B) Evaluation of the activity of ARG-1 FL (0.1 μM) and ARG-1 TR (0.1 μM) at various concentrations of $MnCl_2$. (C) Evaluation of ARG-1 TR and ARG-1 FL thermal stability using nanoDSF (Tycho NT.6.) by diluting the enzyme with and without Mn^{2+} (n = 6). Thermal destabilization of the ARG-1 TR is due to the loss of Mn^{2+}.

p.Arg291*[47,48] and p.Val293*[48] nonsense mutations likely results from impaired ARG-1 oligomerization. To prevent misfolding of the α-helix spanning T285 to F304, we therefore opted to truncate ARG-1 starting from L306, rather than R291 or V293.

Additionally, as reported in the literature,[56] protein stability is often influenced by its oligomeric state, with some proteins showing reduced stability despite maintaining secondary structure.[57−60] This observation led us to explore whether the oligomeric state of the ARG-1 constructs might affect their stability. Our results show that ARG-1 oligomeric state does indeed affect both thermal and chemical stability, as indicated by thermal denaturation (nanoscale differential scanning fluorimetry (nanoDSF); Figure 3E and Table S4) and chemical denaturation (guanidinium.HCl; Table S4) experiments, all without significant changes in secondary structures, as confirmed by CD spectra (Figure 3F).

Next, we measured the affinity of ARG-1 TR and ARG-1 FL for Mn^{2+} by using microscale thermophoresis (MST). To this end, we used *apo*ARG-1 enzymes labeled with a RED-NHS dye and exposed them to increasing concentrations of Mn^{2+}. This study revealed that *apo*ARG-1 FL exhibited higher affinity for Mn^{2+} (K_D = 1.07 [0.49−2.33] μM, Figure 4A) compared to *apo*ARG-1 TR (K_D = 20.16 [14.81−27.45] μM, Figure 4A). We then monitored the activity of ARG-1 FL and ARG-1 TR at various concentrations of Mn^{2+} (Figure 4B and Tables S1, S2, and S3). ARG-1 TR showed some activity at high Mn^{2+} concentration (Mn^{2+} 100 μM: k_{cat}/K_M = 2.3 × 10^3 M^{-1} s^{-1}) but experienced a significant loss in activity at low Mn^{2+} concentrations (Mn^{2+} 0.2 μM: k_{cat}/K_M = 0.3 × 10^3 M^{-1} s^{-1}; Mn^{2+} 1 μM: k_{cat}/K_M = 0.6 × 10^3 M^{-1} s^{-1}). Conversely, ARG-1 FL maintained most of its activity regardless of the Mn^{2+} concentration (Mn^{2+} 0.2 μM: k_{cat}/K_M = 5.7 × 10^3 M^{-1} s^{-1}; Mn^{2+} 1 μM: k_{cat}/K_M = 6.9 × 10^3 M^{-1} s^{-1}; Mn^{2+} 100 μM: k_{cat}/K_M = 7.9 × 10^3 M^{-1} s^{-1}). Finally, the thermal stability of both enzymes was monitored by nanoDSF at various enzyme concentrations with and without Mn^{2+} (Figure 4C). Diluting of ARG-1 TR from 90 to 5 μM resulted in a destabilization of 6.2 °C of the enzyme without Mn^{2+}. This is not observed with Mn^{2+} addition ($\Delta T°_M$ = 0.25 °C after dilution from 90 to 5 μM), confirming that the loss of stability is due to the loss of incorporation of Mn^{2+}. On the other hand, ARG-1 FL is way less affected by dilution, even without Mn^{2+} (destabilization of 1.65 °C after dilution from 90 to 5 μM). These results suggest that monomeric ARG-1 exhibits a lower affinity for Mn^{2+} compared to trimeric ARG-1, potentially explaining the observed loss of activity of the ARG-1 TR. *In silico* analysis showed that Mn^{2+} ions do not interact directly with residues in the truncated C-terminal tail, indicating that mutations or truncations of these residues are unlikely to impact the Mn^{2+}

https://doi.org/10.1021/acs.jmedchem.4c01993
J. Med. Chem. 2025, 68, 1433−1445

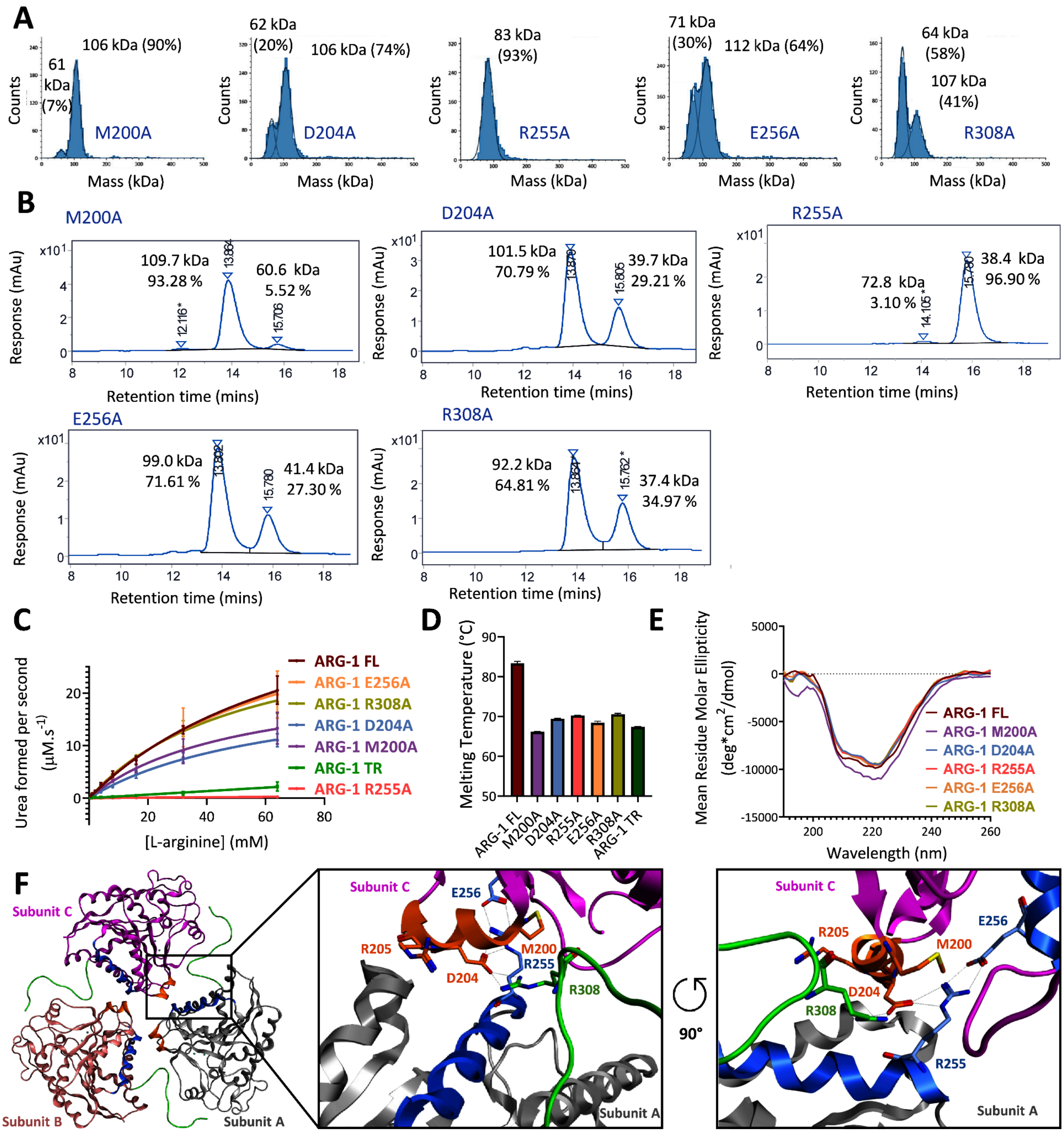

Figure 5. Evaluation of the oligomeric state of the mutants from clusters 1 and 2 to unravel trimerization hotspots. (A) Mass photometry of the mutants (0.05 μM) with the calculated molecular weights of the complex in the solution and their relative intensity indicated above the peaks. (B) SEC-MALS results of ARG-1 M200A, D204A, R255A, E256A, and R308A (25 μM) with the calculated molecular weights of the complex in the solution and their relative intensity indicated above the peaks ($n = 3$) (for molar mass figures: see Figure S5). (C) Evaluation of the mutant activity ($n = 6$). (D) Evaluation of the mutant (10 μM) thermal stability using nanoDSF ($n = 6$). (E) Mutants (0.2 mg/mL) CD spectra. (F) Allosteric pocket identified using site-directed mutagenesis. Subunits A and C are colored respectively in gray and magenta, and clusters 1, 2, and 3 are identified using the MOE software colored in orange, blue, and green, respectively (PDB entry 2AEB).

affinity (Figure S1). This is further supported by the comparable CD spectra obtained for ARG-1 TR and ARG-1 FL (Figure 3F), pointing to affinity differences possibly arising from variations in the oligomeric state. To explore this further, we performed structural studies with site-directed mutagenesis to identify the amino acids essential for trimerization.

Epitope Mapping by Site-Directed Mutagenesis. An alanine scanning was conducted on all amino acids from clusters 1 and 2 (Figure 1), as well as R308 from cluster 3. The latter was used as a control since Lavulo et al. previously reported that this mutation resulted in a monomeric state for ARG-1.[45] The 24 resulting mutants were then fully characterized to determine their oligomeric states, enzyme activity, and thermal/chemical stability. All the mutants were successfully obtained with high purities (Figure S2).

Mass photometry experiments identified five mutants that were mostly or partially monomeric (Figure 5A and Figure S3): ARG-1 M200A (7% monomeric), ARG-1 D204A (20% monomeric), ARG-1 R255A (93% monomeric); ARG-1 E256A (30% monomeric); and ARG-1 R308A (58%

https://doi.org/10.1021/acs.jmedchem.4c01993
J. Med. Chem. 2025, 68, 1433−1445

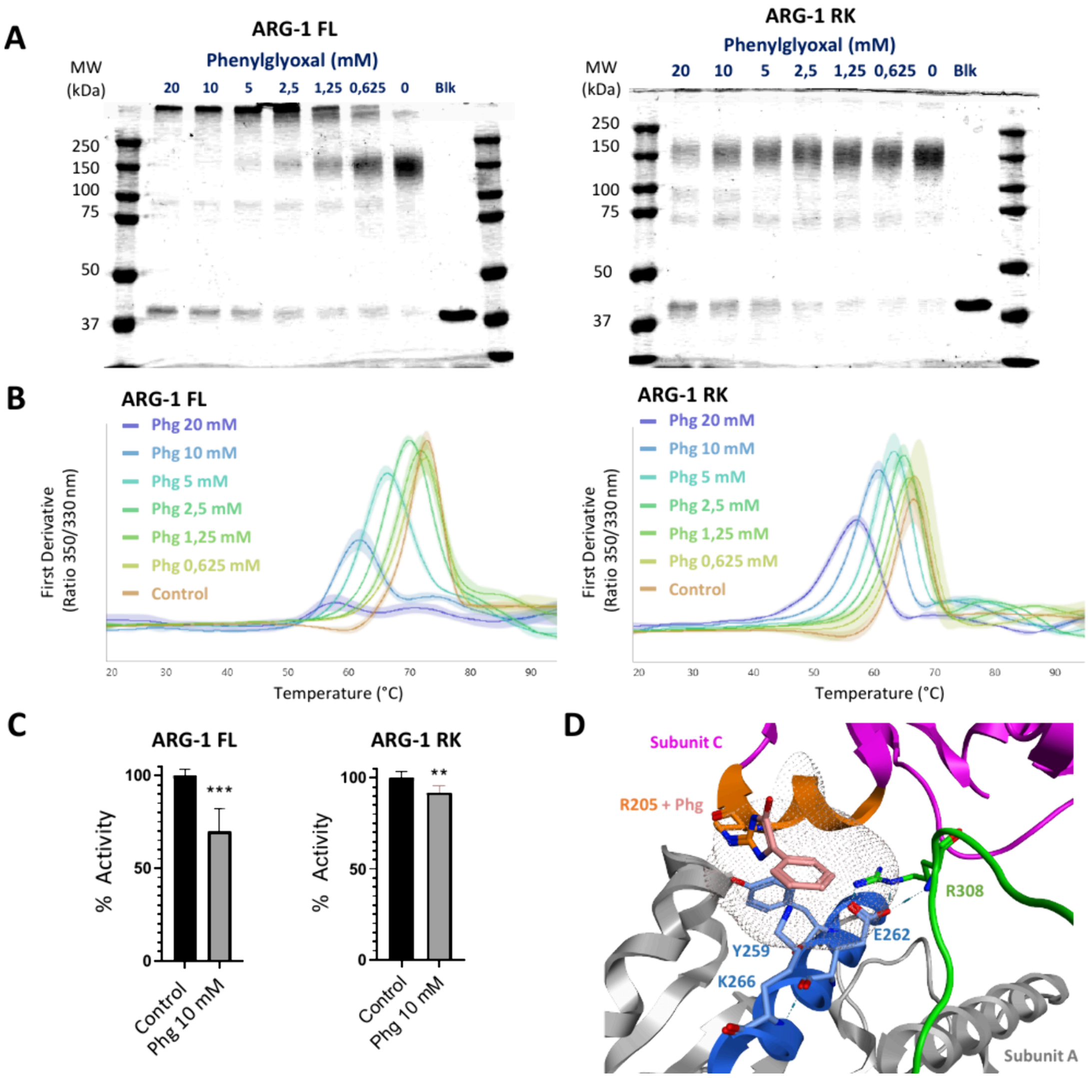

Figure 6. Targeting identifiedL-arginine residues of ARG-1 FL and ARG-1 RK, a mutant conserving L-arginine residues only at the trimeric interface, using phenylglyoxal, a specific covalent binder. (A) Cross-linking experiment with BS^3 0.4 mM after incubation of ARG-1 FL (4 μM) (left) and ARG-1 RK (4 μM) (right) after 24 h of incubation with varying concentrations of phenylglyoxal. (B) Evaluation of ARG-1 FL (5 μM) (left) and ARG-1 RK (5 μM) (right) thermal stability using nanoDSF after 24 h of incubation with varying concentrations of phenylglyoxal ($n = 4$). (C) Evaluation of ARG-1 FL (0.1 μM) (left) and ARG-1 RK (0.1 μM) (right) percentages of activity in physiological conditions after 24 h of incubation with 10 mM of phenylglyoxal ($n = 3$). (D) Mass spectrometry experiments revealed that phenyglyoxal covalently modified R205 (highlighted in light pink), inducing steric clashes (van der Waals surface around the phenylglyoxal adduct computed using the MOE software) with amino acids from clusters 2 (blue) and 3 (green) (PDB entry 2AEB).

monomeric). These findings were corroborated by cross-linking experiments (Figure S4). Further support was provided by SEC-MALS data (Figure 5B and Figure S5): M200A (6% monomeric), D204A (29% monomeric), R255A (97% monomeric), E256A (27% monomeric), and R308A (35% monomeric). Interestingly, the oligomeric state of the five mutants showed a direct correlation with their enzyme activity (Figure 5C and Table S3), thermal stability (Figure 5D and Table S4), and chemical stability (Table S4), with no significant alteration in their secondary structures, as confirmed by CD spectra (Figure 5E). ARG-1 M200A, ARG-1 D204A, ARG-1 R255A, ARG-1 E256A, and ARG-1 R308A exhibit enzyme activities of 75, 53, 1, 76, and 92%, respectively. These findings highlight an allosteric pocket defined by five key residues (Figure 5F), emphasizing the crucial role of these amino acids in the trimerization process and identifying potential new targets for enzyme disruption and inhibition.

Interestingly, the identified allosteric site, derived from the three clusters of interaction predicted *in silico* and confirmed through site-directed mutagenesis, comprises three L-arginine residues: R205, R255, and R308. Notably, R255 stands out as its mutation to an alanine leads to a fully monomeric, inactive mutant, reinforcing our hypothesis that ARG-1 trimerization is essential for enzyme activity. To further validate this hypothesis, we set out to investigate whether a covalent modification of these amino acids with appropriate chemical biology tool compounds could disrupt and, hence, inhibit ARG-1.

Targeting Identified L-Arginine Residues Using a Specific Covalent Binder. To evaluate the potential of targeting the identified allosteric pocket as a novel strategy for ARG-1 inhibition, we employed phenylglyoxal, a covalent modifier known for its selectively toward the guanidinium group of arginine residues.[61] Unlike other vicinal dicarbonyl

https://doi.org/10.1021/acs.jmedchem.4c01993
J. Med. Chem. 2025, 68, 1433−1445

compounds, such as 2,3-butanedione and 1,2-cyclohexanedione,[62−64] phenylglyoxal also exhibits reduced chemical reversibility,[65] enhancing its potential as a covalent modifier for effective ARG-1 disruption. Following a 24 h reaction at 25 °C with phenylglyoxal, the oligomeric state of ARG-1 FL was analyzed by cross-linking experiments (Figure 6A). Remarkably, increasing the phenylglyoxal concentration resulted in a higher proportion of monomeric ARG-1 and a decrease in the trimeric form, leading to a significant 30% loss of enzyme activity (Figure 6C). However, increased aggregation (Figure 6A), likely due to the nonspecific reaction of phenylglyoxal with other solvent exposed L-arginine residues present in ARG-1 FL, was also observed. NanoDSF experiments further revealed that high phenylglyoxal concentrations led to reduced protein stability, complicating conclusions about the phenylglyoxal-specific effect on ARG-1 FL self-assembly (Figure 6B).

To address this, a protein mutant, named ARG-1 RK, retaining only the four L-arginine residues—R180, R205, R255, and R308—positioned at the trimeric interface, with all other solvent-exposed L-arginine residues mutated to L-lysine, was produced (Figure S6A). ARG-1 RK exhibited enzymatic activity under physiological conditions (k_{cat}/K_M = 5.0 × 10^3 M^{-1} s^{-1}; Figure S6B) and maintained a fully trimeric state (115 kDa at 100%; Figure S6C), hence preserving the functional integrity necessary for downstream applications. Following the same protocol, ARG-1 RK was incubated with increasing concentrations of phenylglyoxal, which demonstrated a significant reduction of trimeric ARG-1 RK and an increase in the monomer form without undesired aggregation (cross-linking experiments, Figure 6A). NanoDSF experiments revealed a destabilization of ARG-1 RK upon treatment with increasing concentrations of phenylglyoxal, but it still maintained the profile of a folded protein, even at the highest phenylglyoxal concentration (Figure 6B). Mass spectrometry experiments (Figure S7) indicated that phenylglyoxal would selectively bind to R205. Although the R205A mutation did not affect ARG-1 oligomerization or enzymatic activity (Table S3), the phenylglyoxal adduct likely disrupts critical interactions between two α-helices and R308 via steric hindrance, partially impairing enzyme function (Figure 6D). L-Arginine residues R255 and R308 remained unmodified, probably due to their lower solvent exposure relative to R205. Nevertheless, an 8% decrease in enzyme activity was observed at 10 mM phenylglyoxal (Figure 6C), which aligns with the observation that mutants maintaining a monomer/trimer balance retain most of their activity (Figure 5). The higher inhibition noted in ARG-1 FL versus ARG-1 RK may be attributed to protein aggregation rather than an increased level of trimeric disruption at the allosteric interface. Although phenylglyoxal shows limited inhibitory potency, it illustrates that a small molecule can disrupt ARG-1 oligomerization, thereby reducing its activity. Further optimization of this compound, specifically to enhance interactions with residues R255 and R308, could lead to complete trimer disruption and full enzyme inactivation.

■ CONCLUSIONS

In conclusion, we confirmed that trimerization is essential for the full enzymatic activity of ARG-1 by producing and characterizing both truncated (ARG-1 TR) and full-length (ARG-1 FL) versions of the enzyme. Using orthogonal techniques, such as SEC-MALS, mass photometry, and cross-linking, we established that ARG-1 TR predominantly exists as a monomer, whereas ARG-1 FL forms trimers. Our findings indicate that monomeric ARG-1 TR suffers a significant activity loss of over 90%.

Further investigation into the *apo*-enzymes revealed that the reduced activity of ARG-1 TR is due to its lower affinity for the essential cofactor Mn^{2+}, although Mn^{2+} is not required for trimerization. Through *in silico* studies, we identified an allosteric site involving two α-helices and a C-terminal tail, which governs key subunit−subunit interactions. Site-directed mutagenesis highlighted five critical amino acids—ARG-1 M200, D204, R255, E256, and R308—as essential for ARG-1 self-association, providing essential insights into the molecular basis of ARG-1 trimer formation. Notably, this allosteric pocket is also present in ARG-2 (Figure S8, PDB entry 4HZE), which poses a selectivity challenge for inhibitors. This emphasizes the difficulties to reach selectivity toward the two isoforms of the enzyme.[30] However, selective targeting of extracellular ARG-1 remains feasible, as demonstrated by the reference inhibitor CB-1158, which shows limited cell membrane penetration.[31] Furthermore, dual inhibitors like OATD-02,[66] which have shown antitumor efficacy in animal models, underscore the clinical potential of this approach, since ARG-2 also promotes immunosuppressive effects in tumors.[67]

This allosteric site includes three L-arginine residues: R205, R255, and R308, which were targeted with phenylglyoxal, a covalent modifier selective for arginine. Modification of R205 by phenylglyoxal partially disrupted the trimeric state of ARG-1, likely due to steric clashes with amino acids in the nearby α-helices and R308. Although the inhibitory potency of phenylglyoxal is relatively low, it demonstrates the feasibility of a unique pharmacological approach: disrupting arginase activity by targeting its oligomerization rather than its active site. This small molecule tool validates a promising strategy for arginase inhibition through structural interference.

■ EXPERIMENTAL SECTION

Chemicals and Reagents. All reagents were purchased from chemical suppliers, as specified below, and used without purification.

***In Silico* Evaluation.** Trimeric ARG-1 was generated with the MOE software from the available X-ray crystal structure (PDB entry 2AEB) using the MOE bioassembly tool. Calculation of the free binding energy and mapping of the interactions at ARG-1 interface were performed using the MOE software (ChemComp) with the trimeric ARG-1 (PDB entry 2AEB). The subunit A was set as ligand and the other two as the receptor, and the results were obtained using the Protein Contacts tool. Protein structures were minimized by using the MOE quickprep tool.

Enzymes Production and Quality Evaluation. *Production of ARG-1 FL.* Recombinant *h*ARG-1 gene was inserted in a pET-28a+ plasmid vector ordered from GeneCust. The plasmid was transformed into *Escherichia coli* strain BL21 (DE3) (Rosetta 2) by heat shock. An N-terminal 6-His-tag was added to the sequence of the ARG-1 gene. A single colony of the transformed cells was cultured in terrific broth (TB) medium, supplemented with 50 μg/mL kanamycin and 34 μg/mL chloramphenicol, at 37 °C with an agitation of 120 rpm until an optical density (OD_{600}) of 0.8 was reached. The expression of ARG-1 was induced by 1 mM isopropyl β-d-1-thiogalactopyranoside (IPTG). The culture was grown at 20 °C with agitation at 120 rpm for 20 h. Cells were harvested by centrifugation at 5000 rpm (rotor 11150; Sigma) and 4 °C for 25 min. Cell pellets were resuspended in lysis buffer containing Tris−HCl 50 mM, pH 8.5, $MgCl_2$ 10 mM, $MnCl_2$ 1 mM, NaCl 300 mM, imidazole 5 mM, and glycerol 10% supplemented with cOmplete, EDTA-free protease inhibitor cocktail (Roche) and phenylmethylsulfonyl fluoride 1 mM (PMSF) (Sigma-Aldrich). Cells were disrupted by sonication (6 cycles of 1 min at 4 °C), followed by centrifugation at 10,000 rpm (rotor 12165-H;

https://doi.org/10.1021/acs.jmedchem.4c01993
J. Med. Chem. 2025, 68, 1433−1445

Sigma) and 4 °C for 30 min. The supernatant was collected, supplemented with 15 mM β-mercaptoethanol, and then loaded onto His-trap FF-crude columns (GE Healthcare) according to the manufacturer's instructions for the purification by affinity chromatography. Purified ARG-1 was then dialyzed overnight in a buffer containing Tris−HCl 20 mM, pH 8, NaCl 100 mM, DTT 1 mM, and glycerol 20%. The fraction containing ARG-1 was heated up at 60 °C for 20 min to purify the *holo*-enzyme. The *apo*-enzyme was removed by centrifugation at 10,000 rpm for 30 min (rotor 12165-H; Sigma). Finally, protein concentration was measured using the Bradford method with the Protein Assay Dye Reagent (Bio-Rad), and the sample homogeneity was assessed by SDS-PAGE with InstantBlue Coomassie Protein Stain (Abcam) as a staining agent. To ensure the quality and proper folding of the purified ARG-1, nano differential scanning fluorimetry experiments were performed in the dialysis buffer described above, at 10 μM, on a Tycho NT.6 device (NanoTemper Technologies). Enzyme aliquots were conserved at −80 °C.

Production of ARG-1 TR and Mutants from the Alascan. ARG-1 TR and the mutants were produced and purified following the same procedure as described above for ARG-1 except for the heating step, which was performed only if the enzymes were stable enough to resist thermal degradation.

Production of ApoARG-1 FL and ApoARG-1 TR. *Apo*ARG-1 and *apo*ARG-1tr were produced and purified following the same procedure as described above with the exception of the lysis buffer, which did not contain any $MnCl_2$.

Enzymatic Assays. *Kinetic Assays.* The activity of ARG-1 FL and ARG-1 TR and described mutants was determined following the hydrolysis of radiolabeled L-[guanidino-^{14}C]arginine (American Radiolabeled Chemicals), into L-ornithine and [^{14}C]urea. The assay was adapted from protocols described in the literature.[68] The reaction was performed in a buffer containing sodium phosphate 50 mM, pH 7.4, $MnCl_2$ (0.2; 1 or 100 μM), L-[guanidino-^{14}C]arginine 0.35 μCi/mL and L-arginine concentrations ranging from 0.25 to 64 mM, at a final enzyme concentration of 100 nM, in a total volume of 50 μL, in a 96-well plate (PS, F-Bottom, Clear, Greiner). Samples were incubated for 10 min at 37 °C, and the reaction was stopped by the addition of a 400 μL 1:3 (v/v) Dowex 50W-X8 100−200 (H) (ThermoFisher Scientific) suspension in a stop solution containing acetic acid 0.25 mM, pH 4.5, urea 7 M, and L-arginine 10 mM. Solutions were mixed vigorously by vortex. Samples were then centrifuged at 6000 rpm in a microcentrifuge (rotor 1653, Hettich) for 10 min to pack the Dowex 50W-X8 100−200 (H) resin. 200 μL of the supernatant was carefully removed and mixed with 3 mL of scintillation fluid (Ultima Gold^{TM}, PerkinElmer) for quantification of [^{14}C]urea by scintillation counting using a PerkinElmer counter (model: Tri-Carb 2800TR). Arginase activity, as μmoles of urea formed/min, was calculated as (μmoles L-arginine substrate in the reaction $\times 2.25(A-B))/(C \times T)$, where A is dpm [^{14}C]urea produced in the sample reaction, B is dpm in the blank reaction, C is total dpm L-[guanidino-^{14}C]arginine in reaction, and T is time of incubation in minutes. Total dpm [^{14}C]urea is measured by preparing a sample following the same procedure as described above with the exception of the Dowex 50W-X8 100−200 (H) resin that was avoided. The blank is prepared following the same procedure as described above with the exception that the sample did not contain the enzyme.

Phenylglyoxal Inhibition Assay. 5 μM of purified proteins ARG-1 FL or ARG-1 RK were incubated at 25 °C for 24 h with phenylglyoxal 10 mM in a buffer containing sodium phosphate 50 mM, pH 7.4, NaCl 100 mM, and $MnCl_2$ 100 μM. The reaction mixture was desalted in a buffer containing sodium phosphate 50 mM, pH 7.4, $MnCl_2$ 0.2 μM using Zeba Spin Desalting Columns (ThermoFisher Scientific, 7K MWCO, 0.5 mL), to remove excess phenylglyoxal prior to enzymatic assay. Protein concentration was assessed by using the Bradford Protein Assay Dye Reagent (Bio-Rad). The enzymatic reaction was performed in a buffer containing sodium phosphate 50 mM, pH 7.4, $MnCl_2$ 0.2 μM, L-[guanidino-^{14}C]arginine 0.35 μCi/mL and L-arginine 5 mM, at a final enzyme concentration of 100 nM, in a total volume of 50 μL, in a 96-well plate (PS, F-Bottom, Clear, Greiner). Samples were incubated for 10 min at 37 °C. The reaction was stopped, and the arginase activity was calculated as described above. Results were then expressed as the percent of control activity (sample prepared following the same procedure with the exception that the 24 h incubation is performed without phenylglyoxal).

MST Experiments. MST measurements were performed on a NanoTemper Monolith NT.115 instrument (NanoTemper Technologies). ARG-1 FL was labeled using a red dye-*N*-hydroxysuccinimide second-generation fluorescent dye (NanoTemper Technologies), and ARG-1 TR was labeled using a red dye-*N*-hydroxysuccinimide first-generation fluorescent dye (NanoTemper Technologies), according to the supplier protocol. For ARG-1 FL, measurements were performed in a buffer containing sodium phosphate 50 mM, pH 7.4, NaCl 100 mM, Tween-20 0.05%, and DTT 1 mM in premium-treated capillaries (NanoTemper Technologies). For ARG-1 TR, measurements were performed in a buffer containing sodium phosphate 50 mM, pH 7.4, NaCl 100 mM, Tween-20 0.05%, glycerol 20%, and DTT 1 mM in standard capillaries (NanoTemper Technologies). The final concentration of proteins in the assay was 100 nM. $MnCl_2$ was titrated in 1:1 dilution following the manufacturer's recommendations. Experiments were performed in triplicate using 60% light-emitting diode power, high MST power, laser on time 20 s, and laser off time 3 s. Ligands were evaluated for their thermophoretic pattern, and K_D were extracted from raw data at a 20 s MST on time for ARG-1 FL and at 1.5 s MST on time for ARG-1 TR following the manufacturer's instructions.

Nano Differential Scanning Fluorimetry Experiments. *Protein Evaluation.* Purified proteins ARG-1 and ARG-1 TR and the mutants were diluted at 10 μM in a buffer containing Tris−HCl 50 mM, pH 8, NaCl 100 mM, and glycerol 20% and evaluated on a Tycho NT.6 device (NanoTemper Technologies). According to the standard manufacturer's procedures, samples were poured into capillaries and heated up to 95 °C for 3 min while following fluorescence emission at 330 and 350 nm after excitation at 280 nm. Melting temperatures were extracted from the derivative of the 350/330 nm fluorescence ratios upon increasing the temperature.

Dilution Assay. Purified proteins ARG-1 and ARG-1 TR were diluted at different concentrations (5, 20, 45, and 90 μM) in a buffer containing Tris−HCl 50 mM, pH 8, NaCl 100 mM, and glycerol 20%, with and without 1 mM $MnCl_2$, and evaluated on a Tycho NT.6 device (NanoTemper Technologies). According to the standard manufacturer's procedures, samples were poured into capillaries and heated up to 95 °C for 3 min while following fluorescence emission at 330 and 350 nm after excitation at 280 nm. Melting temperatures were extracted from the derivative of the 350/330 nm fluorescence ratios upon increasing temperature.

Phenylglyoxal Evaluation. 5 μM of purified proteins ARG-1 FL or ARG-1 RK (5 μM) was incubated in a buffer containing sodium phosphate 50 mM, pH 7.4, NaCl 100 mM, and phenylglyoxal at different concentrations (0.625 to 20 mM). A control experiment was performed without the addition of phenylglyoxal. These solutions were evaluated on a Prometheus NT.48 device (NanoTemper Technologies). According to standard manufacturer's procedures, samples were poured into capillaries and heated up from 20 to 95 °C at a heating speed of 1 °C/min while following fluorescence emission at 330 and 350 nm after excitation at 280 nm. Melting temperatures were extracted as the derivative of the 350/330 nm fluorescence ratios upon increasing the temperature.

Cross-Linking Experiments. *Evaluation of Enzyme Oligomeric States.* 4 μM of purified proteins was incubated with BS^3 cross-linker (21580; ThermoFisher) 0.4 mM for 30 min under shaking at 120 rpm at room temperature in a buffer containing sodium phosphate 50 mM, pH 7.4, $MnCl_2$ 100 μM (or without $MnCl_2$ for *apo*-enzyme experiments), and NaCl 100 mM. The reaction was quenched for 15 min with Tris 50 mM, pH 7.5. 2.5 μM of cross-linked protein solutions was mixed with 1× Laemmli sample buffer and DTT 50 mM, boiled for 5 min, and run on SDS/PAGE. Gels were stained with InstantBlue Coomassie Protein Stain (Abcam) overnight.

Phenylglyoxal Evaluation. 9 μM of purified proteins ARG-1 FL or ARG-1 RK was incubated at 25 °C for 24 h with phenylglyoxal at

https://doi.org/10.1021/acs.jmedchem.4c01993
J. Med. Chem. 2025, 68, 1433−1445

concentrations ranging from 0 to 20 mM in a buffer containing sodium phosphate 50 mM, pH 7.4, $MnCl_2$ 100 μM, and NaCl 100 mM. The next steps were as described above.

Chemical Denaturation Experiments. 2 μM purified proteins ARG-1 FL and ARG-1 TR or mutants were incubated with increasing amounts of guanidinium.HCl (final concentrations ranged from 0 to 3 M) for 15 min at room temperature. Fluorescence spectra were recorded afterward at room temperature using an excitation wavelength of 280 nm and recording the emission spectra at 350 nm. Raw fluorescence of every experiment was further subtracted from the corresponding control experiment without the protein.

Mass Photometry Experiments. Protein landing was recorded using a Refeyn One^{MP} (Refeyn Ltd.) MP system by adding 2 μL of the protein stock solution (0.5 μM) directly into an 18 μL drop of filtered buffer containing sodium phosphate 50 mM, pH 7.4, $MnCl_2$ 100 μM (or without $MnCl_2$ for *apo*-enzymes experiments), and NaCl 100 mM. Movies were acquired for 60 s (6000 frames) with the Acquire^{MP} (version 2.1.1; Refeyn Ltd.) software using standard settings. Data were analyzed using default settings on Discover^{MP} (version 2.1.1; Refeyn Ltd.).[69] Contrast-to-mass calibration was performed prior to the experiments using a mixture of proteins with molecular weights of 66, 146, 480, and 1048 kDa.

SEC-UV-MALS-dRI Experiments. SEC-UV-MALS-dRI experiments were performed on a Bio-Inert HPLC system (Agilent 1260 Infinity II, Santa Clara, USA) coupled with a DAD detector (Agilent), a MALS (DAWN8, 658.8 nm), and a dRI (Optilab, 658 nm, 25 °C) detector, both from Wyatt Technology (Dernbach, Germany). The separation was performed on XBridge Premier Protein SEC, 250 Å, 2.5 μm BEH (Ethylene Bridged Hybrid), 4.6 × 300 nm column at 0.2 mL/min equipped with Max Peak Premier Protein SEC Guard, 250 Å, 2.5 μm, 4.6 × 30 mm (both from Waters, Milfort, USA). The column compartment was kept at room temperature. UV absorbance detection was performed at 280 nm. The injection volume was 10 μL. The selected mobile phase condition was made of Tris−HCl 50 mM, pH 7.6, NaCl 150 mM, and $MnCl_2$ 1 mM. $MnCl_2$ was added after adjusting the pH with 1 M HCl. For *apo*ARG-1, $MnCl_2$ was excluded from the mobile phase. The mobile phase was prepared with milli-Q water and filtrated three times using a 0.1 μm PVDF membrane. The Agilent OpenLab CDS C.01.08 (210) software was used for system control and data acquisition, and the UV, MALS, and dRI data were processed in the Astra 8.0.1.21 dedicated software (Wyatt Technology). Band alignment, broadening, and normalization were applied. Protein samples in the stock solutions were diluted to 25 μM in the mobile phase. For all arginase variants, the dn/dc value of 0.186 was applied. The extinction coefficient of 0.64 mL mg^{-1} cm^{-1} was corrected with the experimental value obtained by the software.

LC-MS Experiments. *Sample Preparation.* 6 μM of ARG-1 RK (6 μM) was incubated at 25 °C for 24 h with phenylglyoxal (10 mM) in a buffer containing sodium phosphate 50 mM, pH 7.4, $MnCl_2$ 100 μM, NaCl 100 mM. Samples were run over Zeba Spin Desalting columns 7K MWCO (ThermoFisher) to change buffer to 100 mM sodium hydrogen carbonate. 45 μL samples were then reduced, alkylated, and digested with 50 mM DTT, 50 mM iodoacetamide, and 0.2 mg/mL trypsin/Lys-C, respectively. Samples were evaporated with speed vac and resuspended in 10% acetonitrile with 0.1% formic acid.

LC-Chip-DTIMS-Q-TOF Conditions. The LC experiments were performed on a 1200-series system from Agilent Technologies composed of a capillary pump, a nanoflow pump, an autosampler, and a Chipcube acting as LC-Chip/MS interface. The separation was carried out on an ultrahigh-capacity LC-Chip according to ref 70. This fully integrated system is composed of a 500 nL enrichment column, a 150 mm × 75 μm ID analytical column, a six-port switching valve, and a nanospray emitter tip. Both columns were packed with a Zorbax C18 phase (5 μm particle size). Mobile phases A and B were composed of H_2O/FA (99.9:0.1, v/v) and ACN/H_2O/FA (90:10:0.1, v/v), respectively. The compositions are the same for both capillary and nanoflow pumps. The peptides were first loaded in the trapping column at 3 μL min^{-1} in isocratic mode (97:3, v/v). After valve switching, the peptides were backflushed from the trapping column into the separation column by the nanoflow pump at a flow rate of 300 nL min^{-1}. The gradient elution of the peptides was performed as follows: 0−10 min, 3% B; 10−13 min, from 3 to 8% B; 13−73 min, from 8 to 38% B; 73−78 min, from 38 to 90% B; 78−93 min, 90% B; 93−98 min, from 90 to 3% B; and 98−110 min, 3% B. The injection volume was set at 2 μL. The MS experiments were performed on a 6560 hybrid ion mobility Q-TOF (Agilent Technologies) in positive electrospray ionization mode. Nitrogen was used as drying gas at 4 L min^{-1} and 300 °C. Reference masses (purine and HP-921) were added onto an absorptive wick located in the Chipcube. Data-dependent acquisition (DDA) rates for precursor and product ions were set at 8 and 5 Hz, respectively. Precursor selection criteria for fragmentation were set as follows: intensity threshold: 3000 counts; relative threshold: 0.001%; peptides as isotope models; isolation width: 4 amu; maximum 15 precursors per cycle; active exclusion after one spectrum during 0.3 min was enabled. The application of the collision energy was determined using the following formula: for doubly charged ions, slope: 3.1; offset: −6.6; for triply charged ions: slope: 3.6; offset: −12.4; for more than triply charged ions: slope: 3.6; offset: −12.4. Instrument control and data acquisitions were all achieved through MassHunter Workstation Data Acquisition software (Version B.09.00).

Data Treatment and Protein Identification. For the DDA analyses, raw data files were processed using the Spectrum Mill software (Agilent Technologies). The peptides were identified by searching in the Homemade database using the following parameters: carbamidomethylation of cysteines as fixed modifications, oxidation of methionines and deamidation as the variable modifications, 25% minimum matched peak intensity, 20 ppm precursor mass tolerance, 50 ppm product mass tolerance, and trypsin/Lys-C digestion enzyme with a maximum of two missed cleavages. The reversed database score calculation and dynamic peak thresholding were used. Only the peptides having a score higher than five and a scored peak intensity (SPI) higher than 60% were kept for data analysis.

CD Experiments. Purified proteins ARG-1, *apo*ARG-1, and ARG-1 TR and the five mutants (M200A, D204A, R255A, E256A, and R308A) were initially stored in a buffer containing Tris−HCl 50 mM, pH 8, NaCl 100 mM, and glycerol 20%. Samples were run over Zeba Spin Desalting columns 7K MWCO (ThermoFisher) to change buffer to potassium phosphate 20 mM, pH 7.4, NaF 100 mM. Protein concentration was measured using the Bradford method with the Protein Assay Dye Reagent (Bio-Rad) and diluted in the phosphate buffer to reach a protein concentration of 0.2 mg/mL. CD measurements were performed using a BioLogic MOS-500 CD spectropolarimeter (BioLogic, France) at 25 °C in a quartz cuvette with a 1 mm path length (no. 110-1-40; Hellma Analytics). Far UV spectra (190 to 260 nm) were recorded at a scan speed of 50 nm/min and a 1 nm bandwidth. Ten spectra were measured and averaged. The CD spectra were plotted by using GraphPad Prism.

■ ASSOCIATED CONTENT

Data Availability Statement

All raw data supporting the findings of this study are available from the corresponding author upon request

Supporting Information

The Supporting Information is available free of charge at https://pubs.acs.org/doi/10.1021/acs.jmedchem.4c01993.

Protein purity assessed by SDS-PAGE; mass photometry and cross-linking results; SEC-MALS results associated with the molar mass figures; superposition of the identified allosteric pocket of ARG-1 and the corresponding pocket in ARG-2; ARG-1 RK enzymatic activity and SEC-MALS results; MS/MS analysis; tables presenting the kinetic parameters, thermal stability and chemical stability of all proteins assessed (PDF)

AUTHOR INFORMATION

Corresponding Author

Raphaël Frédérick – *Louvain Drug Research Institute (LDRI), Medicinal Chemistry Research Group (CMFA), Université Catholique de Louvain (UCLouvain), Brussels B-1200, Belgium;* orcid.org/0000-0001-8119-1272; Email: raphael.frederick@uclouvain.be

Authors

Juhans Dechenne – *Louvain Drug Research Institute (LDRI), Medicinal Chemistry Research Group (CMFA), Université Catholique de Louvain (UCLouvain), Brussels B-1200, Belgium;* orcid.org/0009-0004-9486-6880

Magdalena Wierzbicka – *Laboratory for the Analysis of Medicines (CIRM), Université de Liège (ULG), Liège B-4000, Belgium*

Reda Krimou – *Louvain Drug Research Institute (LDRI), Medicinal Chemistry Research Group (CMFA), Université Catholique de Louvain (UCLouvain), Brussels B-1200, Belgium*

Asia El Aakchioui – *Louvain Drug Research Institute (LDRI), Medicinal Chemistry Research Group (CMFA), Université Catholique de Louvain (UCLouvain), Brussels B-1200, Belgium*

Julia Malo Pueyo – *VIB-VUB Center for Structural Biology, Vlaams Instituut Voor Biotechnologie, Brussels B-1050, Belgium; Brussels Center for Redox Biology and Structural Biology Brussels, Vrije Universiteit Brussel, Brussels B-1050, Belgium*

Joris Messens – *VIB-VUB Center for Structural Biology, Vlaams Instituut Voor Biotechnologie, Brussels B-1050, Belgium; Brussels Center for Redox Biology and Structural Biology Brussels, Vrije Universiteit Brussel, Brussels B-1050, Belgium*

Marianne Fillet – *Laboratory for the Analysis of Medicines (CIRM), Université de Liège (ULG), Liège B-4000, Belgium;* orcid.org/0000-0002-1453-6282

Quentin Spillier – *Louvain Drug Research Institute (LDRI), Medicinal Chemistry Research Group (CMFA), Université Catholique de Louvain (UCLouvain), Brussels B-1200, Belgium*

Complete contact information is available at: https://pubs.acs.org/10.1021/acs.jmedchem.4c01993

Author Contributions

J.D. and R.F. designed the research. J.D., M.W., A.E., R.K., and G.C. performed the research experiments. J.D., J.M., and M.W. analyzed the data. J.D., J.M.P., and M.W. set up the experimental methods. J.D., Q.S., M.F., J.M., and R.F. wrote the paper.

Notes

The authors declare no competing financial interest.

ACKNOWLEDGMENTS

This work was supported by the Belgian Fonds National de la Recherche Scientifique (F.R.S.- FNRS Grant T008223F and the French Community of Belgium (ARC 21/26-115). The authors thank Gael Cobraiville for his contribution to the LC-MS experiments.

ABBREVIATIONS

ARG, arginase; ARG-1, arginase-1; ARG-1 FL, arginase-1 full length; ARG-1 TR, arginase-1 truncated; ARG-1 RK, arginase-1 with solvent exposed L-arginine mutated into L-lysines; ITPG, isopropyl β-d-1-thiogalactopyranoside; MDSC, myeloid-derived suppressor cell; MST, microscale thermophoresis; nanoDSF, nano differential scanning fluorimetry; NHS, *N*-hydroxysuccinimide; Phg, phenylglyoxal; PMSF, phenylmethylsulfonyl fluoride; SEC-MALS, size-exclusion chromatography coupled with multiangle light scattering; TB, terrific broth

REFERENCES

(1) Grzywa, T. M.; Sosnowska, A.; Matryba, P.; Rydzynska, Z.; Jasinski, M.; Nowis, D.; Golab, J. Myeloid Cell-Derived Arginase in Cancer Immune Response. *Front Immunol* **2020**, *11* (May), 938.

(2) Christianson, D. W. Arginase: structure, mechanism, and physiological role in male and female sexual arousal. *Acc. Chem. Res.* **2005**, *38* (3), 191–201.

(3) Caldwell, R. W.; Rodriguez, P. C.; Toque, H. A.; Narayanan, S. P.; Caldwell, R. B. Arginase: A Multifaceted Enzyme Important in Health and Disease. *Physiol Rev.* **2018**, *98* (2), 641–665.

(4) Bagnost, T.; Ma, L.; da Silva, R. F.; Rezakhaniha, R.; Houdayer, C.; Stergiopulos, N.; Andre, C.; Guillaume, Y.; Berthelot, A.; Demougeot, C. Cardiovascular effects of arginase inhibition in spontaneously hypertensive rats with fully developed hypertension. *Cardiovasc. Res.* **2010**, *87* (3), 569–577.

(5) Chen, B.; Calvert, A. E.; Cui, H.; Nelin, L. D. Hypoxia promotes human pulmonary artery smooth muscle cell proliferation through induction of arginase. *Am. J. Physiol Lung Cell Mol. Physiol* **2009**, *297* (6), L1151–1159.

(6) Bakshi, N.; Morris, C. R. The role of the arginine metabolome in pain: implications for sickle cell disease. *J. Pain Res.* **2016**, *9*, 167–175.

(7) Bagi, Z.; Feher, A.; Dou, H.; Broskova, Z. Selective up-regulation of arginase-1 in coronary arteries of diabetic patients. *Front Immunol* **2013**, *4*, 293.

(8) Gonon, A. T.; Jung, C.; Katz, A.; Westerblad, H.; Shemyakin, A.; Sjoquist, P. O.; Lundberg, J. O.; Pernow, J. Local arginase inhibition during early reperfusion mediates cardioprotection via increased nitric oxide production. *PLoS One* **2012**, *7* (7), No. e42038.

(9) Berkowitz, D. E.; White, R.; Li, D.; Minhas, K. M.; Cernetich, A.; Kim, S.; Burke, S.; Shoukas, A. A.; Nyhan, D.; Champion, H. C.; Hare, J. M. Arginase reciprocally regulates nitric oxide synthase activity and contributes to endothelial dysfunction in aging blood vessels. *Circulation* **2003**, *108* (16), 2000–2006.

(10) Cox, J. D.; Kim, N. N.; Traish, A. M.; Christianson, D. W. Arginase-boronic acid complex highlights a physiological role in erectile function. *Nat. Struct. Biol.* **1999**, *6* (11), 1043–1047.

(11) Petrone, A. B.; O'Connell, G. C.; Regier, M. D.; Chantler, P. D.; Simpkins, J. W.; Barr, T. L. The Role of Arginase 1 in Post-Stroke Immunosuppression and Ischemic Stroke Severity. *Transl Stroke Res.* **2016**, *7* (2), 103–110.

(12) Hansmannel, F.; Sillaire, A.; Kamboh, M. I.; Lendon, C.; Pasquier, F.; Hannequin, D.; Laumet, G.; Mounier, A.; Ayral, A. M.; DeKosky, S. T.; et al. Is the urea cycle involved in Alzheimer's disease? *J. Alzheimers Dis* **2010**, *21* (3), 1013–1021.

(13) Cantoni, C.; Cignarella, F.; Ghezzi, L.; Mikesell, B.; Bollman, B.; Berrien-Elliott, M. M.; Ireland, A. R.; Fehniger, T. A.; Wu, G. F.; Piccio, L. Mir-223 regulates the number and function of myeloid-derived suppressor cells in multiple sclerosis and experimental autoimmune encephalomyelitis. *Acta Neuropathol* **2017**, *133* (1), 61–77.

(14) Elms, S. C.; Toque, H. A.; Rojas, M.; Xu, Z.; Caldwell, R. W.; Caldwell, R. B. The role of arginase I in diabetes-induced retinal vascular dysfunction in mouse and rat models of diabetes. *Diabetologia* **2013**, *56* (3), 654–662.

(15) Bron, L.; Jandus, C.; Andrejevic-Blant, S.; Speiser, D. E.; Monnier, P.; Romero, P.; Rivals, J. P. Prognostic value of arginase-II expression and regulatory T-cell infiltration in head and neck squamous cell carcinoma. *Int. J. Cancer* **2013**, *132* (3), E85−93.

(16) Ma, Z.; Lian, J.; Yang, M.; Wuyang, J.; Zhao, C.; Chen, W.; Liu, C.; Zhao, Q.; Lou, C.; Han, J.; Zhang, Y. Overexpression of Arginase-1 is an indicator of poor prognosis in patients with colorectal cancer. *Pathol Res. Pract* **2019**, *215* (6), No. 152383.

(17) Czystowska-Kuzmicz, M.; Sosnowska, A.; Nowis, D.; Ramji, K.; Szajnik, M.; Chlebowska-Tuz, J.; Wolinska, E.; Gaj, P.; Grazul, M.; Pilch, Z.; et al. Small extracellular vesicles containing arginase-1 suppress T-cell responses and promote tumor growth in ovarian carcinoma. *Nat. Commun.* **2019**, *10* (1), 3000.

(18) Ren, W.; Zhang, X.; Li, W.; Feng, Q.; Feng, H.; Tong, Y.; Rong, H.; Wang, W.; Zhang, D.; Zhang, Z.; Tu, S. Circulating and tumor-infiltrating arginase 1-expressing cells in gastric adenocarcinoma patients were mainly immature and monocytic Myeloid-derived suppressor cells. *Sci. Rep* **2020**, *10* (1), 8056.

(19) Mussai, F.; Egan, S.; Hunter, S.; Webber, H.; Fisher, J.; Wheat, R.; McConville, C.; Sbirkov, Y.; Wheeler, K.; Bendle, G.; et al. Neuroblastoma Arginase Activity Creates an Immunosuppressive Microenvironment That Impairs Autologous and Engineered Immunity. *Cancer Res.* **2015**, *75* (15), 3043−3053.

(20) Mussai, F.; De Santo, C.; Abu-Dayyeh, I.; Booth, S.; Quek, L.; McEwen-Smith, R. M.; Qureshi, A.; Dazzi, F.; Vyas, P.; Cerundolo, V. Acute myeloid leukemia creates an arginase-dependent immunosuppressive microenvironment. *Blood* **2013**, *122* (5), 749−758.

(21) de Boniface, J.; Mao, Y.; Schmidt-Mende, J.; Kiessling, R.; Poschke, I. Expression patterns of the immunomodulatory enzyme arginase 1 in blood, lymph nodes and tumor tissue of early-stage breast cancer patients. *Oncoimmunology* **2012**, *1* (8), 1305−1312.

(22) Rotondo, R.; Barisione, G.; Mastracci, L.; Grossi, F.; Orengo, A. M.; Costa, R.; Truini, M.; Fabbi, M.; Ferrini, S.; Barbieri, O. IL-8 induces exocytosis of arginase 1 by neutrophil polymorphonuclears in nonsmall cell lung cancer. *Int. J. Cancer* **2009**, *125* (4), 887−893.

(23) Li, J. H.; Zhang, S. Q.; Qiu, X. G.; Zhang, S. J.; Zheng, S. H.; Zhang, D. H. Long non-coding RNA NEAT1 promotes malignant progression of thyroid carcinoma by regulating miRNA-214. *Int. J. Oncol.* **2017**, *50* (2), 708−716.

(24) Andrade, L. N. S.; Otake, A. H.; Cardim, S. G. B.; da Silva, F. I.; Ikoma Sakamoto, M. M.; Furuya, T. K.; Uno, M.; Pasini, F. S.; Chammas, R. Extracellular Vesicles Shedding Promotes Melanoma Growth in Response to Chemotherapy. *Sci. Rep* **2019**, *9* (1), 14482.

(25) You, J.; Chen, W.; Chen, J.; Zheng, Q.; Dong, J.; Zhu, Y. The Oncogenic Role of ARG1 in Progression and Metastasis of Hepatocellular Carcinoma. *BioMed Res. Int.* **2018**, *2018*, No. 2109865.

(26) Rodriguez, P. C.; Ernstoff, M. S.; Hernandez, C.; Atkins, M.; Zabaleta, J.; Sierra, R.; Ochoa, A. C. Arginase I-producing myeloid-derived suppressor cells in renal cell carcinoma are a subpopulation of activated granulocytes. *Cancer Res.* **2009**, *69* (4), 1553−1560.

(27) Sippel, T. R.; White, J.; Nag, K.; Tsvankin, V.; Klaassen, M.; Kleinschmidt-DeMasters, B. K.; Waziri, A. Neutrophil degranulation and immunosuppression in patients with GBM: restoration of cellular immune function by targeting arginase I. *Clin. Cancer Res.* **2011**, *17* (22), 6992−7002.

(28) Bronte, V.; Serafini, P.; Mazzoni, A.; Segal, D. M.; Zanovello, P. L-arginine metabolism in myeloid cells controls T-lymphocyte functions. *Trends Immunol.* **2003**, *24* (6), 301−305.

(29) Borek, B.; Gajda, T.; Golebiowski, A.; Blaszczyk, R. Boronic acid-based arginase inhibitors in cancer immunotherapy. *Bioorg. Med. Chem.* **2020**, *28* (18), No. 115658.

(30) Failla, M.; Molaro, M. C.; Schiano, M. E.; Serafini, M.; Tiburtini, G. A.; Gianquinto, E.; Scoccia, R.; Battisegola, C.; Rimoli, M. G.; Chegaev, K.; et al. Opportunities and Challenges of Arginase Inhibitors in Cancer: A Medicinal Chemistry Perspective. *J. Med. Chem.* **2024**, *67* (22), 19988−20021.

(31) Steggerda, S. M.; Bennett, M. K.; Chen, J.; Emberley, E.; Huang, T.; Janes, J. R.; Li, W.; MacKinnon, A. L.; Makkouk, A.; Marguier, G.; et al. Inhibition of arginase by CB-1158 blocks myeloid cell-mediated immune suppression in the tumor microenvironment. *J. Immunother Cancer* **2017**, *5* (1), 101.

(32) Nishi, H.; Hashimoto, K.; Madej, T.; Panchenko, A. R. Evolutionary, physicochemical, and functional mechanisms of protein homooligomerization. *Prog. Mol. Biol. Transl Sci.* **2013**, *117*, 3−24.

(33) Thabault, L.; Liberelle, M.; Frederick, R. Targeting protein self-association in drug design. *Drug Discov Today* **2021**, *26* (5), 1148−1163.

(34) Wells, S. A.; van der Kamp, M. W.; McGeagh, J. D.; Mulholland, A. J. Structure and Function in Homodimeric Enzymes: Simulations of Cooperative and Independent Functional Motions. *PLoS One* **2015**, *10* (8), No. e0133372.

(35) Levy, E. D.; Pereira-Leal, J. B.; Chothia, C.; Teichmann, S. A. 3D complex: a structural classification of protein complexes. *PLoS Comput. Biol.* **2006**, *2* (11), No. e155.

(36) Jubb, H. C.; Pandurangan, A. P.; Turner, M. A.; Ochoa-Montano, B.; Blundell, T. L.; Ascher, D. B. Mutations at protein-protein interfaces: Small changes over big surfaces have large impacts on human health. *Prog. Biophys. Mol. Biol.* **2017**, *128*, 3−13.

(37) Anastassiadis, T.; Deacon, S. W.; Devarajan, K.; Ma, H.; Peterson, J. R. Comprehensive assay of kinase catalytic activity reveals features of kinase inhibitor selectivity. *Nat. Biotechnol.* **2011**, *29* (11), 1039−1045.

(38) Gunderwala, A. Y.; Nimbvikar, A. A.; Cope, N. J.; Li, Z.; Wang, Z. Development of Allosteric BRAF Peptide Inhibitors Targeting the Dimer Interface of BRAF. *ACS Chem. Biol.* **2019**, *14* (7), 1471−1480.

(39) Kubota, H. Quality control against misfolded proteins in the cytosol: a network for cell survival. *J. Biochem* **2009**, *146* (5), 609−616.

(40) Joshi, R. G.; Kulkarni, S.; Ratna Prabha, C. Engineering degrons of yeast ornithine decarboxylase as vehicles for efficient targeted protein degradation. *Biochim. Biophys. Acta* **2015**, *1850* (12), 2452−2463.

(41) Pi, F.; Vieweger, M.; Zhao, Z.; Wang, S.; Guo, P. Discovery of a new method for potent drug development using power function of stoichiometry of homomeric biocomplexes or biological nanomotors. *Expert Opin Drug Deliv* **2016**, *13* (1), 23−36.

(42) Kanyo, Z. F.; Scolnick, L. R.; Ash, D. E.; Christianson, D. W. Structure of a unique binuclear manganese cluster in arginase. *Nature* **1996**, *383* (6600), 554−557.

(43) Sabio, G.; Mora, A.; Rangel, M. A.; Quesada, A.; Marcos, C. F.; Alonso, J. C.; Soler, G.; Centeno, F. Glu-256 is a main structural determinant for oligomerisation of human arginase I. *FEBS Lett.* **2001**, *501* (2−3), 161−165.

(44) Lobos, M.; Figueroa, M.; Martinez-Oyanedel, J.; Lopez, V.; Garcia-Robles, M. L. A.; Tarifeno-Saldivia, E.; Carvajal, N.; Uribe, E. Insights on the participation of Glu256 and Asp204 in the oligomeric structure and cooperative effects of human arginase type I. *J. Struct Biol.* **2020**, *211* (2), No. 107533.

(45) Lavulo, L. T.; Sossong, T. M., Jr.; Brigham-Burke, M. R.; Doyle, M. L.; Cox, J. D.; Christianson, D. W.; Ash, D. E. Subunit-subunit interactions in trimeric arginase. Generation of active monomers by mutation of a single amino acid. *J. Biol. Chem.* **2001**, *276* (17), 14242−14248.

(46) Carvalho, D. R.; Brand, G. D.; Brum, J. M.; Takata, R. I.; Speck-Martins, C. E.; Pratesi, R. Analysis of novel ARG1 mutations causing hyperargininemia and correlation with arginase I activity in erythrocytes. *Gene* **2012**, *509* (1), 124−130.

(47) Grody, W. W.; Klein, D.; Dodson, A. E.; Kern, R. M.; Wissmann, P. B.; Goodman, B. K.; Bassand, P.; Marescau, B.; Kang, S. S.; Leonard, J. V.; et al. Molecular genetic study of human arginase deficiency. *Am. J. Hum. Genet.* **1992**, *50* (6), 1281−1290.

(48) Scholl-Bürgi, S.; Baumgartner Sigl, S.; Häberle, J.; Haberlandt, E.; Rostásy, K.; Ertl, C.; Eichinger-Öttl, U.; Heinz-Erian, P.; Karall, D. Amino acids in CSF and plasma in hyperammonaemic coma due to arginase1 deficiency. *J. Inherited Metab. Dis.* **2008**, *31*, 323−328.

(49) Lawrence, S. H.; Ramirez, U. D.; Tang, L.; Fazliyez, F.; Kundrat, L.; Markham, G. D.; Jaffe, E. K. Shape shifting leads to

small-molecule allosteric drug discovery. *Chem. Biol.* **2008**, *15* (6), 586−596.

(50) McMillan, K.; Adler, M.; Auld, D. S.; Baldwin, J. J.; Blasko, E.; Browne, L. J.; Chelsky, D.; Davey, D.; Dolle, R. E.; Eagen, K. A.; et al. Allosteric inhibitors of inducible nitric oxide synthase dimerization discovered via combinatorial chemistry. *Proc. Natl. Acad. Sci. U. S. A.* **2000**, *97* (4), 1506−1511.

(51) Meng, B.; Wu, D.; Gu, J.; Ouyang, S.; Ding, W.; Liu, Z. J. Structural and functional analyses of human tryptophan 2,3-dioxygenase. *Proteins* **2014**, *82* (11), 3210−3216.

(52) Ziebarth, T. D.; Gonzalez-Soltero, R.; Makowska-Grzyska, M. M.; Nunez-Ramirez, R.; Carazo, J. M.; Kaguni, L. S. Dynamic effects of cofactors and DNA on the oligomeric state of human mitochondrial DNA helicase. *J. Biol. Chem.* **2010**, *285* (19), 14639−14647.

(53) Wu, D.; Piszczek, G. Standard protocol for mass photometry experiments. *Eur. Biophys J.* **2021**, *50* (3−4), 403−409.

(54) Chen, P.; Bornhorst, J.; Aschner, M. Manganese metabolism in humans. *Front Biosci (Landmark Ed)* **2018**, *23* (9), 1655−1679.

(55) Slordahl, T. S.; Hov, H.; Holt, R. U.; Baykov, V.; Syversen, T.; Sundan, A.; Waage, A.; Borset, M. Mn2+ regulates myeloma cell adhesion differently than the proadhesive cytokines HGF, IGF-1, and SDF-1alpha. *Eur. J. Haematol* **2008**, *81* (6), 437−447.

(56) Miller, S.; Lesk, A. M.; Janin, J.; Chothia, C. The accessible surface area and stability of oligomeric proteins. *Nature* **1987**, *328* (6133), 834−836.

(57) Gokhale, R. S.; Agarwalla, S.; Francis, V. S.; Santi, D. V.; Balaram, P. Thermal stabilization of thymidylate synthase by engineering two disulfide bridges across the dimer interface. *J. Mol. Biol.* **1994**, *235* (1), 89−94.

(58) Thoma, R.; Hennig, M.; Sterner, R.; Kirschner, K. Structure and function of mutationally generated monomers of dimeric phosphoribosylanthranilate isomerase from Thermotoga maritima. *Structure* **2000**, *8* (3), 265−276.

(59) Lunev, S.; Butzloff, S.; Romero, A. R.; Linzke, M.; Batista, F. A.; Meissner, K. A.; Muller, I. B.; Adawy, A.; Wrenger, C.; Groves, M. R. Oligomeric interfaces as a tool in drug discovery: Specific interference with activity of malate dehydrogenase of Plasmodium falciparum in vitro. *PLoS One* **2018**, *13* (4), No. e0195011.

(60) Seetoh, W. G.; Abell, C. Disrupting the Constitutive, Homodimeric Protein-Protein Interface in CK2beta Using a Biophysical Fragment-Based Approach. *J. Am. Chem. Soc.* **2016**, *138* (43), 14303−14311.

(61) Takahashi, K. Further studies on the reactions of phenylglyoxal and related reagents with proteins. *J. Biochem* **1977**, *81* (2), 403−414.

(62) Oya, T.; Hattori, N.; Mizuno, Y.; Miyata, S.; Maeda, S.; Osawa, T.; Uchida, K. Methylglyoxal modification of protein. Chemical and immunochemical characterization of methylglyoxal-arginine adducts. *J. Biol. Chem.* **1999**, *274* (26), 18492−18502.

(63) Patthy, L.; Smith, E. L. Reversible modification of arginine residues. Application to sequence studies by restriction of tryptic hydrolysis to lysine residues. *J. Biol. Chem.* **1975**, *250* (2), 557−564.

(64) Yankeelov, J. A., Jr.; Mitchell, C. D.; Crawford, T. H. A simple trimerization of 2,3-butanedione yielding a selective reagent for the modification of arginine in proteins. *J. Am. Chem. Soc.* **1968**, *90* (6), 1664−1666.

(65) Riordan, J. F. Arginyl residues and anion binding sites in proteins. *Mol. Cell. Biochem.* **1979**, *26* (2), 71−92.

(66) Grzybowski, M. M.; Stanczak, P. S.; Pomper, P.; Blaszczyk, R.; Borek, B.; Gzik, A.; Nowicka, J.; Jedrzejczak, K.; Brzezinska, J.; Rejczak, T.; et al. OATD-02 Validates the Benefits of Pharmacological Inhibition of Arginase 1 and 2 in Cancer. *Cancers* **2022**, *14* (16), 3967.

(67) Dunand-Sauthier, I.; Irla, M.; Carnesecchi, S.; Seguin-Estevez, Q.; Vejnar, C. E.; Zdobnov, E. M.; Santiago-Raber, M. L.; Reith, W. Repression of arginase-2 expression in dendritic cells by microRNA-155 is critical for promoting T cell proliferation. *J. Immunol* **2014**, *193* (4), 1690−1700.

(68) Kepka-Lenhart, D.; Ash, D. E.; Morris, S. M. Determination of mammalian arginase activity. *Methods Enzymol* **2008**, *440* (07), 221−230.

(69) Young, G.; Hundt, N.; Cole, D.; Fineberg, A.; Andrecka, J.; Tyler, A.; Olerinyova, A.; Ansari, A.; Marklund, E. G.; Collier, M. P.; et al. Quantitative mass imaging of single biological macromolecules. *Science* **2018**, *360* (6387), 423−427.

(70) Nys, G.; Cobraiville, G.; Fillet, M. Multidimensional performance assessment of micro pillar array column chromatography combined to ion mobility-mass spectrometry for proteome research. *Anal. Chim. Acta* **2019**, *1086*, 1−13.

https://doi.org/10.1021/acs.jmedchem.4c01993
J. Med. Chem. 2025, 68, 1433−1445